

CFD Simulation for Cavitation of Propeller Blade

Dr. O. O. Sulaiman¹

¹ Universiti Malaysia Terengganu.

Received: 8 December 2011 Accepted: 31 December 2011 Published: 15 January 2012

Abstract

Propeller cavitation is a major problem in ship operation and the costs of repair and maintenance is high for ship-owners. Proper design of propeller plays a very important role in life cycle and the performance of a vessel. The use of simulation to observe various parameters that affect cavitations can be helpful to optimize propeller performance. This project designs and simulates cavitations flow of a Kaplan series, Fixed Pitch Propeller (FPP) of a 48-metres Multipurpose Deck Ship at 11 knots. Simulation test was carried out for laminar and turbulent flow using Computational Fluid Dynamics (CFD) approach to observe cavitations occurrence at selected radius. The parameters considered are pitch angle, angle of attack, viscosity of sea water, operating vapour pressure in the sea water, engine power, lift and drag vectors of each of the blade sections, and resultant velocity of the fluid flow. Comparison of performance is made and it compares well with the theory. Thrust coefficient (KT), torque coefficient (KQ), thrust (T), advance coefficient (J), and cavitations number (?), were calculated to deduce efficiency and validate the model. The study can be used to build a prototype physical model that could be beneficial for future additional experimentation investigation.

Index terms— Simulation, cavitation, performance, propeller, CFD.

1 Introduction

marine propeller is a propulsion system which turns the power delivered by the engine into thrust to drive the vessel through water. Propeller cavitation is a general problem encountered by the ship owner, whereby it causes vibrations, noises, degradation of propeller performance, deceases engine efficiencies, effects the life cycle of the ship and also results in high cost of maintenance. The basic physics of cavitation occurs when the pressure of liquid is lower or equal to the vapour pressure, which depends on the temperature, thus forming cavities or bubbles. The compression of pressure surrounding the cavities would break the cavities into smaller parts and this increases the temperature. Collapse of bubbles in contact with parts of the propeller blades will create high localised forces that subsequently erode the surface of the blades. Simulation on cavitating flow using CFD can be carried out to determine the performance of the propeller. A model is generated in Gambit and fluid-flow physics are applied to predict the fluid dynamics and other physical phenomena related to the propeller. Ref. [1] stated that, CFD can provide potential flow analysis such as flow velocities and pressure at every point in the problem domain as well as the inclusion of viscous effects. a) Previous studies on propeller cavitation Ref. [2] in their studies, generated hybrid grid of about 187 000 cells using Gambit and T Grid. The blade surface was firstly meshed with triangles including the root, tip and blade edges. The turbulent boundary layer was resolved with four layers of prismatic cells between blade and hub surfaces. In the cavitating propeller case, the boundary conditions were set to simulate the flow around a rotating propeller in open water. Inlet boundary, velocity components for uniform stream, blade and hub surfaces, and outer boundary were included. This ensured the rotational periodicity of the propeller on the exit boundary by setting the pressure corresponding to the given cavitation number and other variables was later extrapolated [3,11]. On the other hand, [3] applied a mixture of models with algebraic slip to simulate cavitating flow over a NACA 66 hydrofoil. This multiphase flow model which used incompressible fluids

44 consisting of liquid and vapour was used as primary and secondary phase respectively. Structured quadrilateral
 45 grids of 19 490 cells were meshed. Inflow and outflow boundary were indicated as velocity magnitude and direction
 46 and zero gauge pressure respectively. Contour of vapour volume fraction shown in Figure 1 indicates that cavity
 47 can be observed at the mid-chord region [4,12]. This study is focussed mainly on simulating a cavitating flow at
 48 the propeller blade section of Kaplan series in order to optimize the propeller blade to increase its performance.
 49 Two-dimensional simulations of different radii were carried out at different revolutions per minute (rpm) and the
 50 results were compared based on the pressure difference. The objective is to simulate and investigate the water
 51 flow at the propeller blade A section and to recommend measures to reduce cavitation in order to increase its
 52 efficiencies [4,5].

53 2 II.

54 3 Methodology a) Model generation in Gambit

55 The Propeller Blade models of 0.2R and 0.6R were generated and computational domains were created to assume
 56 water is flowing from far towards the Propeller Blade. Figure 2 and Table ?? show far-field boundary conditions
 57 surrounding the Propeller Blade. Then, meshing was carried out between the boundaries and Propeller Blade to
 58 determine the accuracy of the model generation. Figure ?? and 4 show the meshing process [6,13,14]. Propeller
 59 blades of 0.2R and 0.6R were simulated in Fluent 6.3.26. Pressure-based numerical solver, laminar and turbulent
 60 physical model were selected as the functioning base for 300rpm and 600rpm. Then, the material properties, for
 61 instance, the density of sea water and viscosity value were defined and calculated based on Table 2.. Consequently,
 62 the operating condition was set to be 2296 Pa, which is the condition for vapour pressure at sea water when the
 63 temperature is 20°C. On the other hand, the boundary conditions of far field 1 and far field 2 were specified as
 64 velocity inlet, whereby the velocity magnitude and direction were calculated [??, ??].

65 As for far field 3, this boundary was specified as pressure outlet; the gauge pressure was set to be 0 Pa. The
 66 existence of inflow and outflow boundaries enables the characteristics of fluid to be observed by entering and
 67 leaving the flow domain. The turbulent viscosity ratio was set to correspond to the default value for 600rpm of
 68 both radii. Next, the solution procedure was set as simple algorithm, and under discretisation, the pressure and
 69 momentum were set as Standard and First Order Upwind respectively [??,10].

70 4 Dynamic viscosity = kinematic viscosity x density (1)

71 Therefore, the calculated dynamic viscosity is 1.08035×10^{-9} kg/m.s.

72 Consequently, the operating condition was set to be 2296 Pa based on Table 3, which is the condition for
 73 vapour pressure at sea water when the temperature is 20°C. On the other hand, the boundary conditions of far
 74 field 1, far field 2 and far field 3 were specified to accommodate the fluid behaviour. Far field 1 and far field 2
 75 were specified as velocity-inlet, whereby the velocity magnitude and direction were calculated as the following:

76 For 0.2R airfoil section profile, Pitch angle, $\theta = \tan^{-1} (P/2r)$, (2) where, P is pitch and r is radius of the
 77 blade section Thus, resultant velocity of the fluid flow at 0.2R is calculated as, Resultant velocity, $v = (2rn \cos \theta)$, (3)

79 Where, n is equal to the rotational speed of the propeller Resultant velocity, $v = (2rn \cos \theta)$, (4)

80 Velocity-inlets at both far fields were then indicated as 729 m/s for 0.2R airfoil section. As for far field 3, this
 81 boundary was specified as pressure-outlet, whereby the gauge pressure was set to be zero Pascal. The existence of
 82 inflow and outflow boundaries enables the characteristics of fluid to be observed by entering and leaving the flow
 83 domain. Parameters in the solution control were set up to select the suitable iterative solvers. Under pressure-
 84 velocity coupling, the solution procedure was set as SIMPLE algorithm, which equipped an accurate linkage
 85 between pressure and velocity. SIMPLE algorithm was used due to the assumption of steady flows. Besides,
 86 under discretization, the pressure and momentum were set as Standard and First Order Upwind respectively. The
 87 First Order Upwind was set due to convection terms in solution, thus the face value would be set to cell-centre
 88 value. This was done before any CFD calculation was performed. The solution was then initialised and computed
 89 from far field 1.

90 Monitoring of the convergence of the solution was performed. There were three differential equations to
 91 be solved in a two-dimensional incompressible laminar flow problem, which indicated the three residuals to be
 92 monitored for convergence, that is, continuity, x-velocity and y-velocity. The default convergence criteria were
 93 set as 0.001 for all three of these. As the code iterates, the residuals were calculated for each flow of equation.
 94 These residuals represented an average error in the solution. Moreover, monitoring lift and drag force was carried
 95 out and calculated as following: For 0.2R airfoil section profile, Angle of attack, $\theta = (2f_{max} C)$ (5)

96 Where, f_{max} is thickness of the airfoil section and C is chord length of the airfoil section Angle of attack, $\theta =$
 97 $(2f_{max} C)$ (6) Lift force is defined as a force perpendicular to the direction of the freestream. Therefore, X and
 98 Y are formulated as $\sin \theta$ and negative $\cos \theta$, respectively, as shown in Figure 5. As for the drag force vector, it
 99 is defined as the force component in the direction of the freestream.

100 Thus, X and Y are formulated as negative $\cos \theta$ and $\sin \theta$ respectively, as shown in Figure 6. Therefore, lift
 101 force vectors at X and Y were -0.5736 and 0.819 respectively.

102 The solution was solved and iterated in order to remove the unwanted accumulations, so that the iterative
 103 process would converge rather than diverge. A converge solution is usually achieved when the residuals fall below

104 some convergence criteria, that is 0.001. Besides examining residuals, variables such as lift and drag force were
105 monitored to find out the convergence of the numerical computations.

106 Last but not least, the CFD results were visualised and analysed at the end of the computational simulation
107 in different categories, such as vector plots and contour plots for a better relevant physical characteristics view
108 within the fluid -flow problem.

109 The simulation process was repeated by inserting various operating pressure values below 2296 Pa in order
110 to observe the pressure difference for cavitation to occur and also to examine the sensitivity for accuracy of the
111 results and performance. Finally, document the findings of the analysis.

112 5 III.

113 6 Results and Discussions

114 Three Propeller Blade section profiles at different radii, such as 0.2R, 0.6R and 1.0R were simulated. The CFD
115 results were then visualised and analysed for comparison. 6, it can be seen that the residuals were moving upwards
116 and not fulfilling the converging criteria, that is to be below 0.001. This shows that the solution was diverging
117 instead of converging. As for the lift and drag vector force, Figure ?? and 9 shows a divergence result which is
118 not compatible with the convergence criteria. For 0.6R Propeller Blade section, the CFD results, for instance,
119 three residuals of CFD calculation, lift and drag force, velocity vector plot, and contour plot were visualised
120 and analysed (Figure 11). f) Iteration of 0.6R Figure 14 shows 250 iteration results, whereby the continuity, x-
121 velocity and y-velocity were calculated for flow equation. It can be seen that the residuals were moving downwards
122 equivalent to the convergence criteria, which is 0.001. This shows that the solution was converging. Based on
123 the above contours, cavitations can happen if the Propeller Blade radius section increases, especially for 0.6R
124 compared to 0.2R. This is because the bigger the radius, themore pressure would be concentrated at that location.
125 Besides this, in the turbulent flow, cavitation is more likely to be induce compared to laminar flow due to its
126 fluid characteristics. Also, the higher the rpm, the lower the absolute pressure.

127 7 g) Graph of absolute pressure versus curve length

128 The graph in Figure 19 shows that, the pressure decreases when it passes by the Propeller Blade equivalent to
129 the diagrams shown above and as it leaves the Propeller Blade, the pressure slowly increases back to its actual
130 pressure. Figure 20 shows cavitation number, ? versus advance coefficient, based on the graph. When the
131 propeller rotates at 300rpm, the operating condition falls in the region for a conventional propeller, which is
132 suitable for most of the merchant vessels, whereas, at 600rpm, propeller operating condition falls in the poor
133 region for high -speed propeller operation. This indicates low efficiency for propeller since low advance coefficient
134 implies high propeller power coefficient. This is probably due to inaccurate application of propeller rotational
135 speed with engine load and gear box used.

136 When the propeller rotates at 300rpm, the advance coefficient and cavitation number reaches the region for
137 conventional propeller operation. This means that, at 300rpm, the propeller rotates at a good condition suitable
138 to the engine load and gear box required. On the other hand, when the propeller rotates at higher speed, it
139 reaches a poor region for highspeed propeller operation which indicates damages, vibration and cavitation would
140 occur. Based on the results of velocity and contour plots of 300rpm and 600rpm, the higher the rpm, the lower
141 the absolute pressure, which is the condition for cavitation to occur. This is caused by high rotational rates of the
142 propeller which creates high -pressure and low-pressure region on the blades. Besides, when the radius increases
143 along the propeller, cavitation might happen too. Airfoil section profile at 0.2R does not have cavitation due to
144 less pressure concentration in that region compared to 0.6R airfoil section profile. At 0.6R airfoil section profile,
145 more works is required to be done in that region [14, ???].

146 8 IV.

147 9 Conclusion

148 The paper presents the result of water flow at the blade section profile. Cavitation occurrence is observed to be
149 at the upper surface of 0.6R compared to 0.2R of propeller blade section due to different pressure concentrations.
150 Besides, cavitation is predicted at low absolute pressure when the rpm is high and this correlates with theory
151 hypothesis. Optimisation of the propeller can be achieved by increasing the blade area ratio (BAR) and compare it
152 with the standard Kaplan BAR value that is, 0.85. The result deduced from this study can be added to existing
153 databased for validation purposes especially for ship navigating within Malaysian water. This could provide
154 information on environmental differential impact on propeller. It is recommended that further multiphase,
155 experimental simulation should carried out to test rotational speed of propeller at different powers produced by
156 the engine load.

157 V.



Figure 1: Figure 1 :



Figure 2: Figure 2 :

134

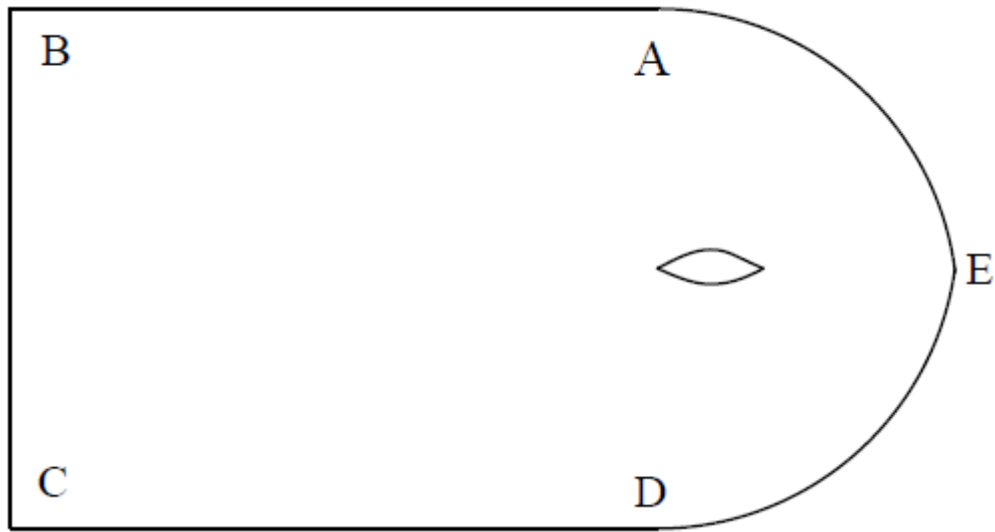


Figure 3: Table 1 :Figure 3 :Figure 4 :

Curve	Boundary condition
AED	Far field 1
AB	Far field 2
CD	Far field 2
BC	Far field 3

5

Figure 4: Figure 5 :

6

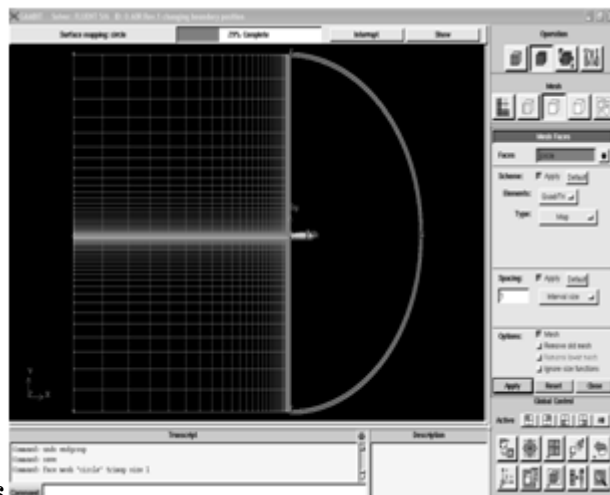


Figure 5: Figure 6 :

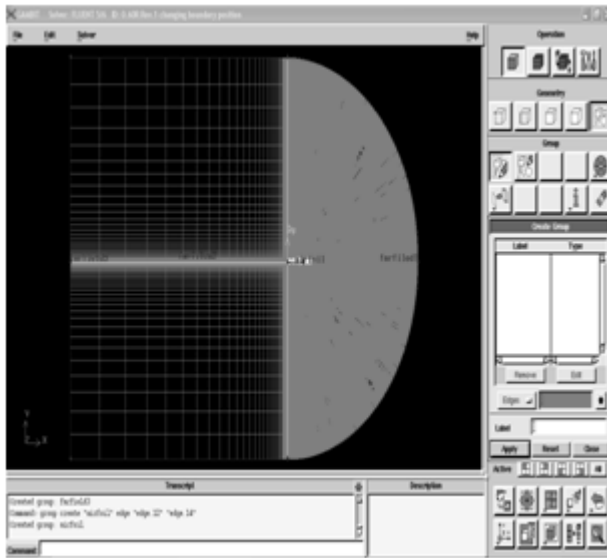


Figure 6:

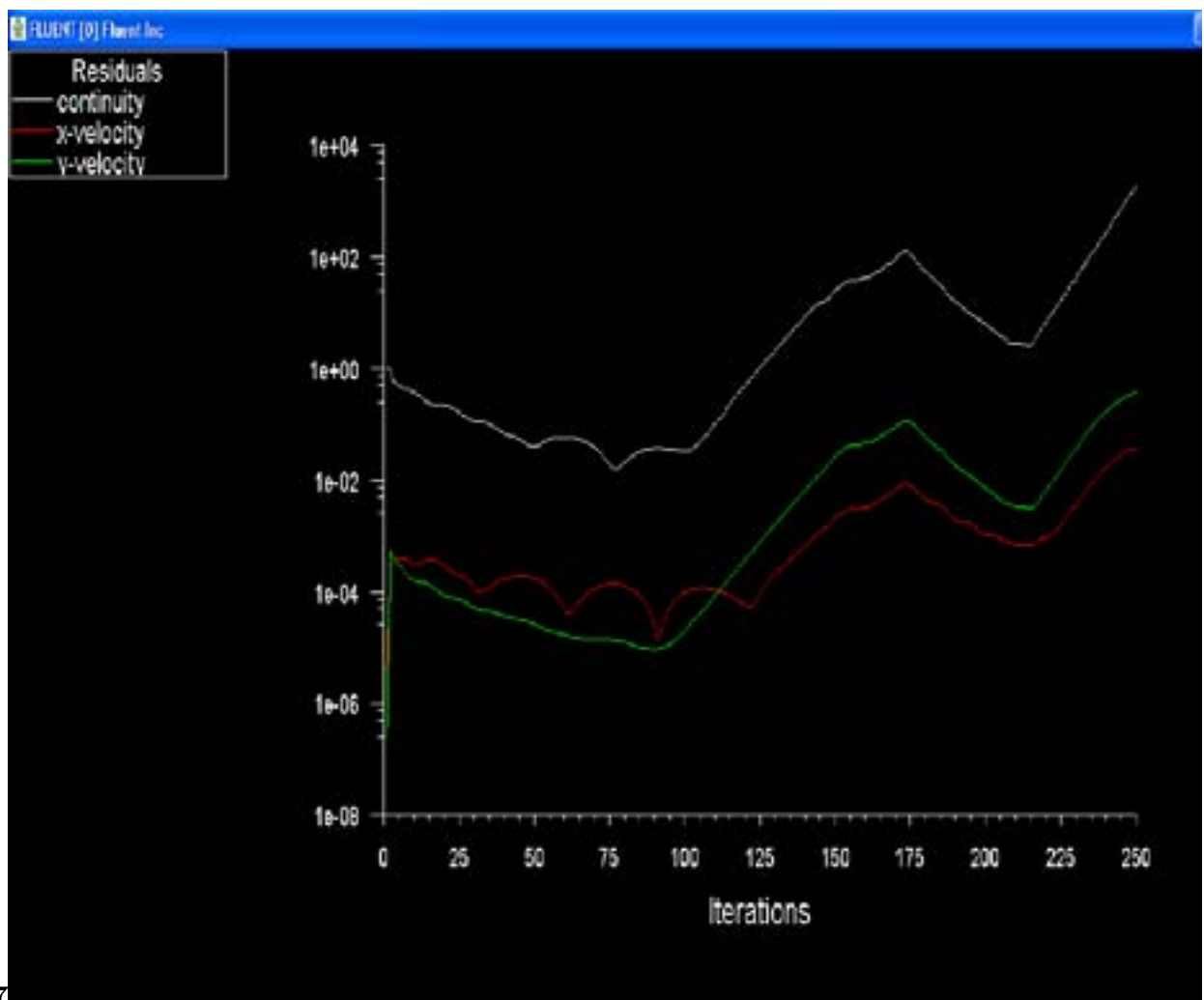


Figure 7: Figure 7 :

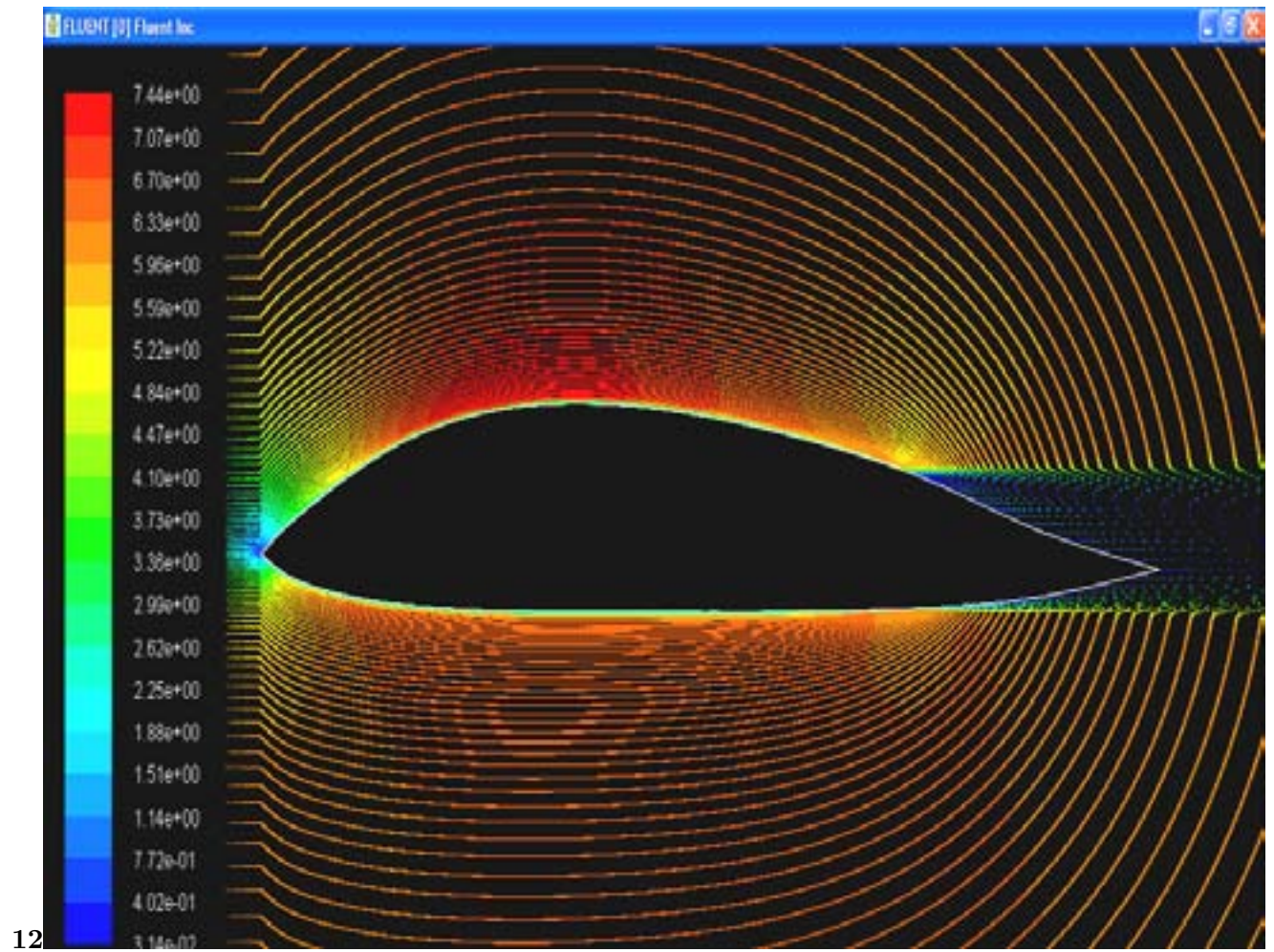


Figure 10: Figure 12 :

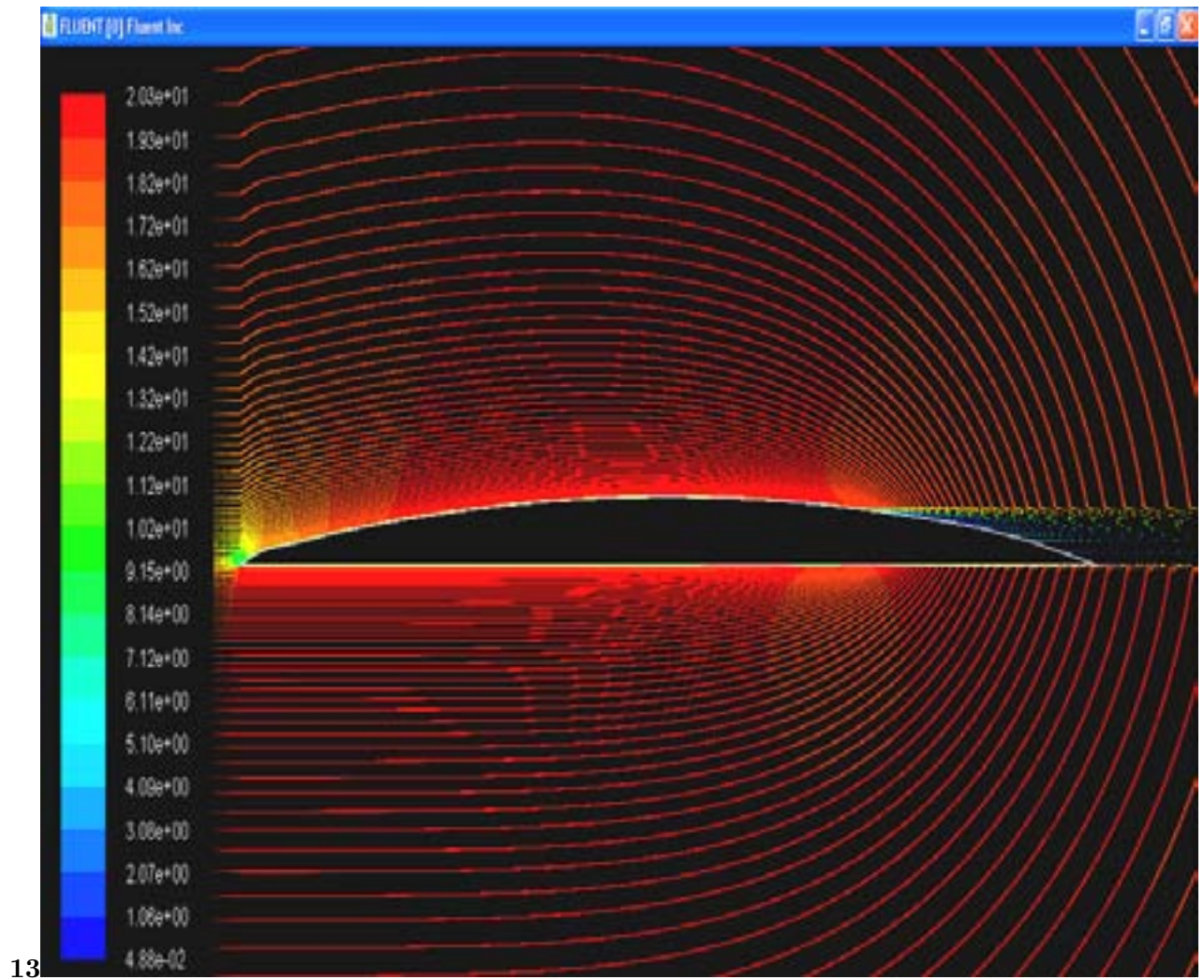


Figure 11: Figure 13 :

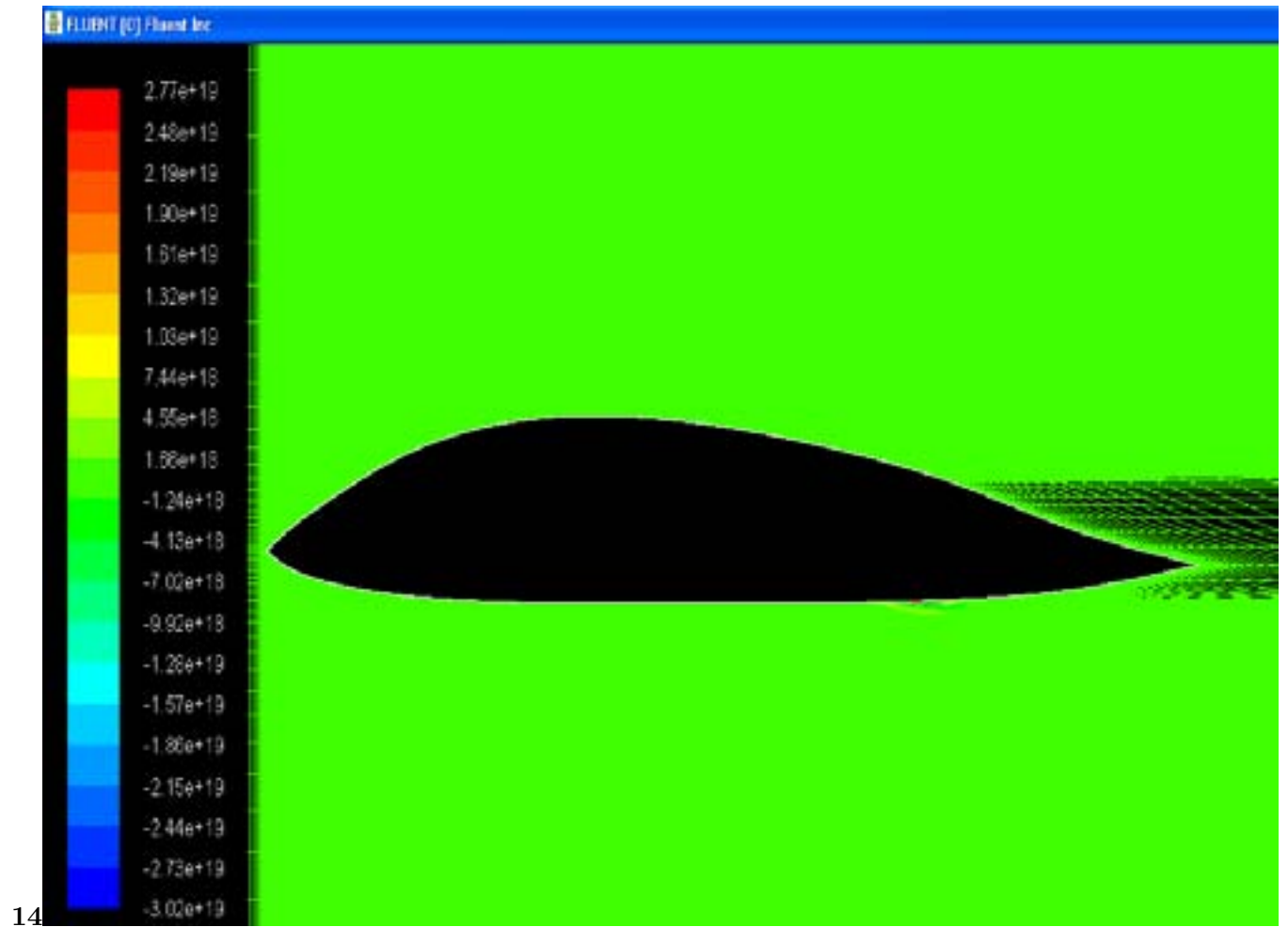
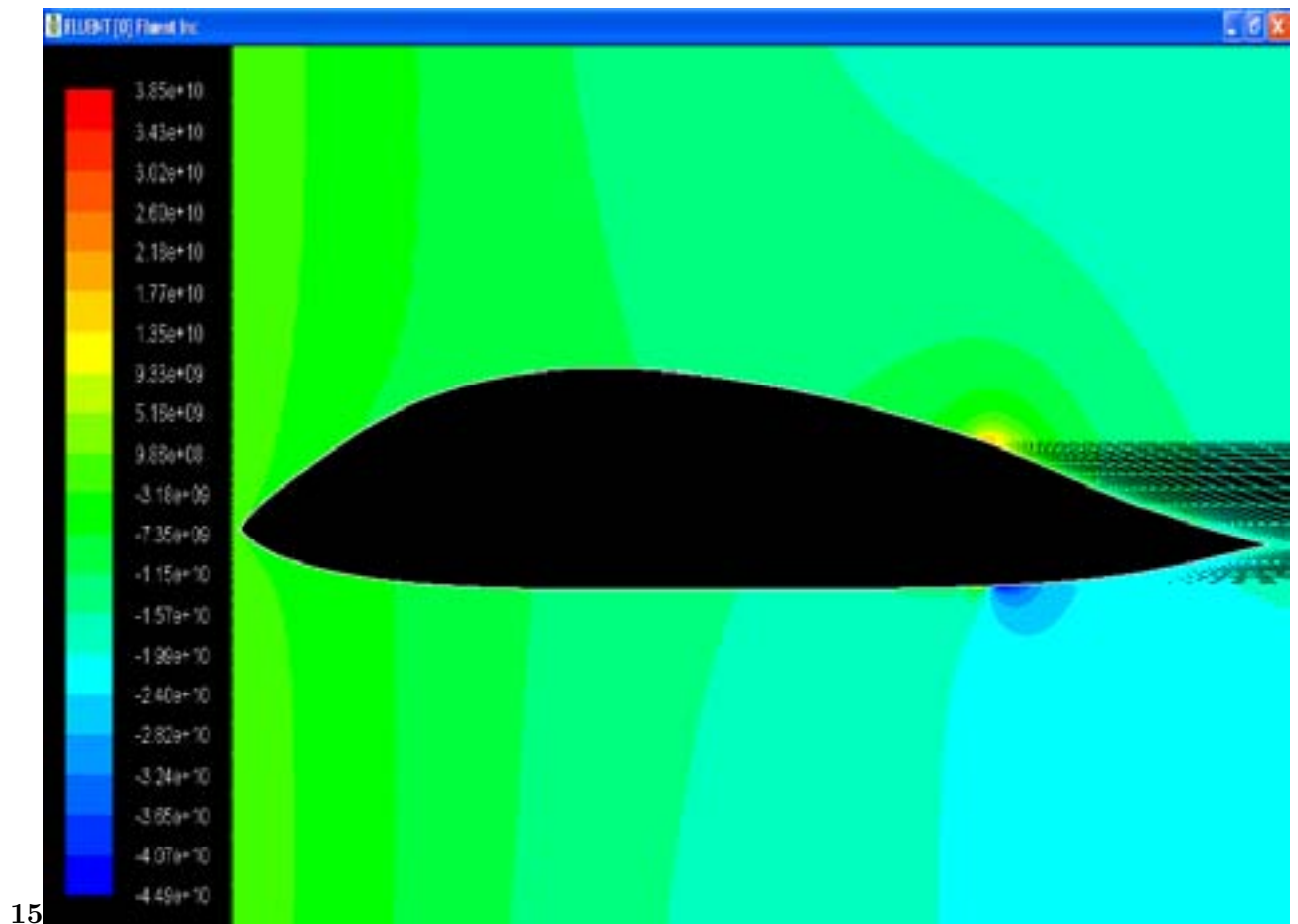


Figure 12: Figure 14 :



15

Figure 13: Figure 15 :

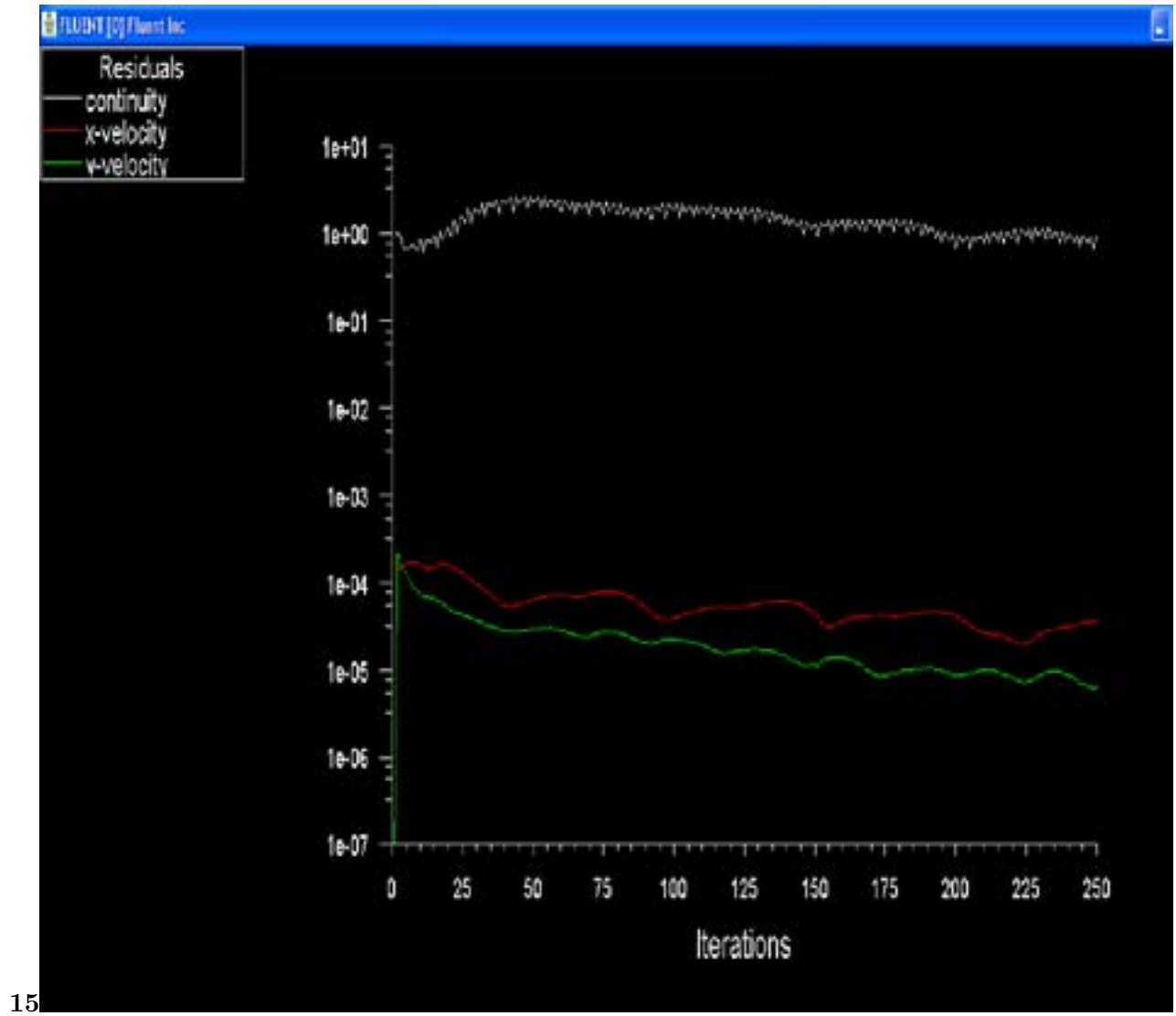


Figure 14: Figure 15 :

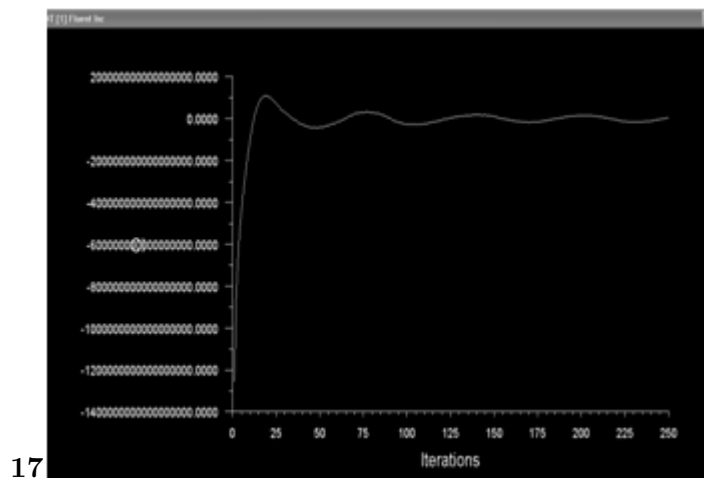


Figure 15: Figure 17 :

18

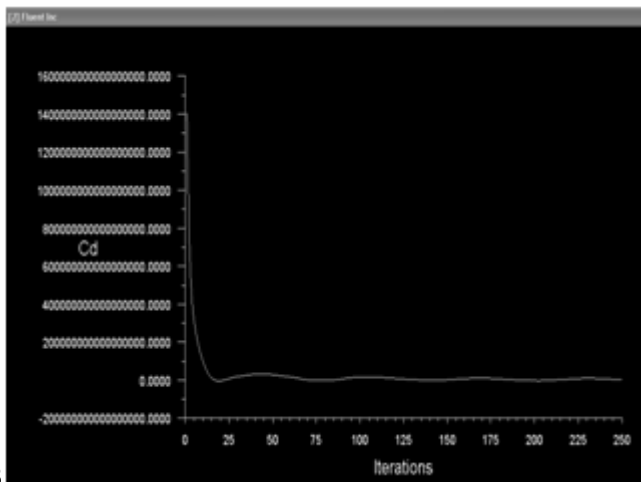


Figure 16: Figure 18 :

19

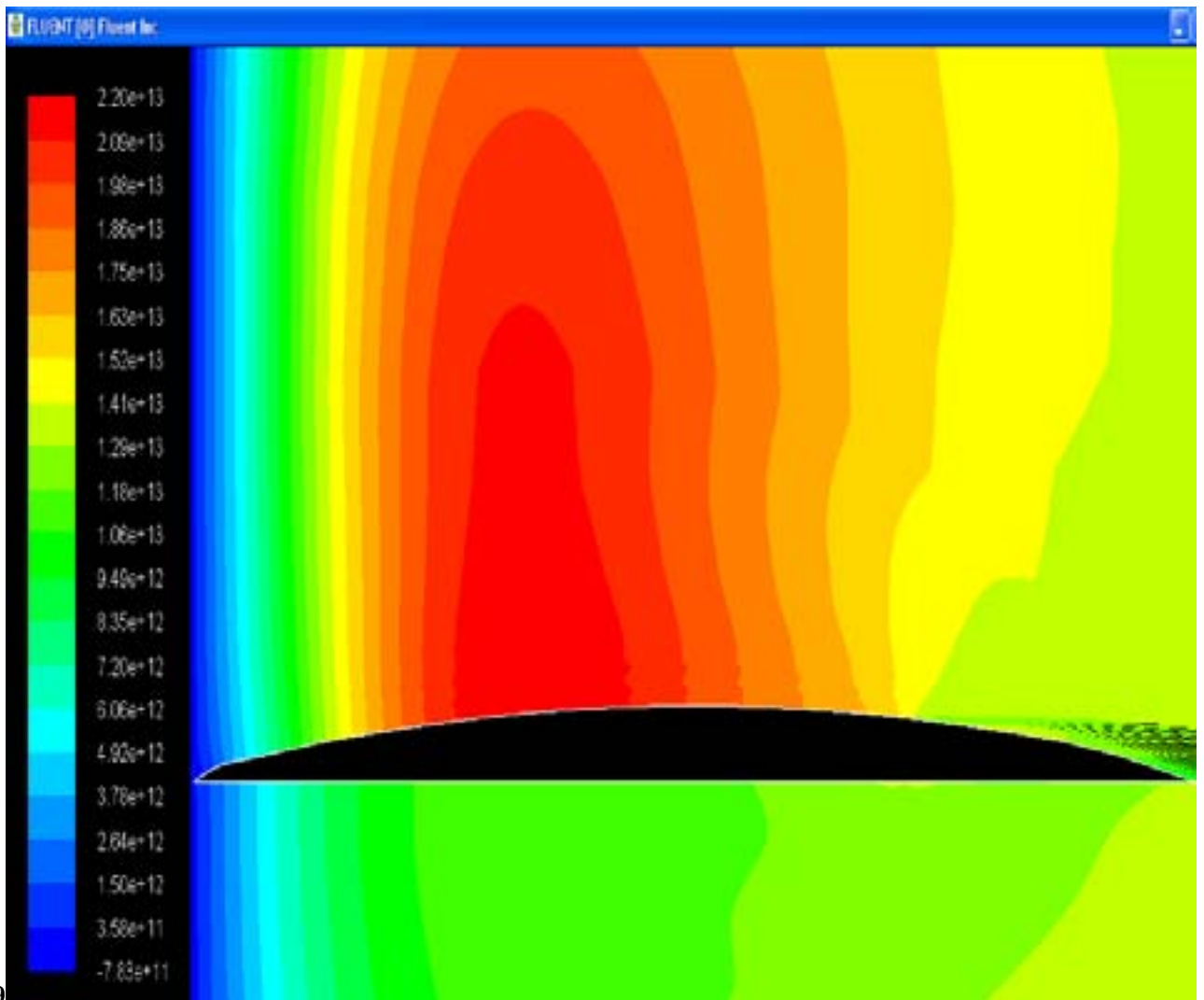


Figure 17: Figure 19 :

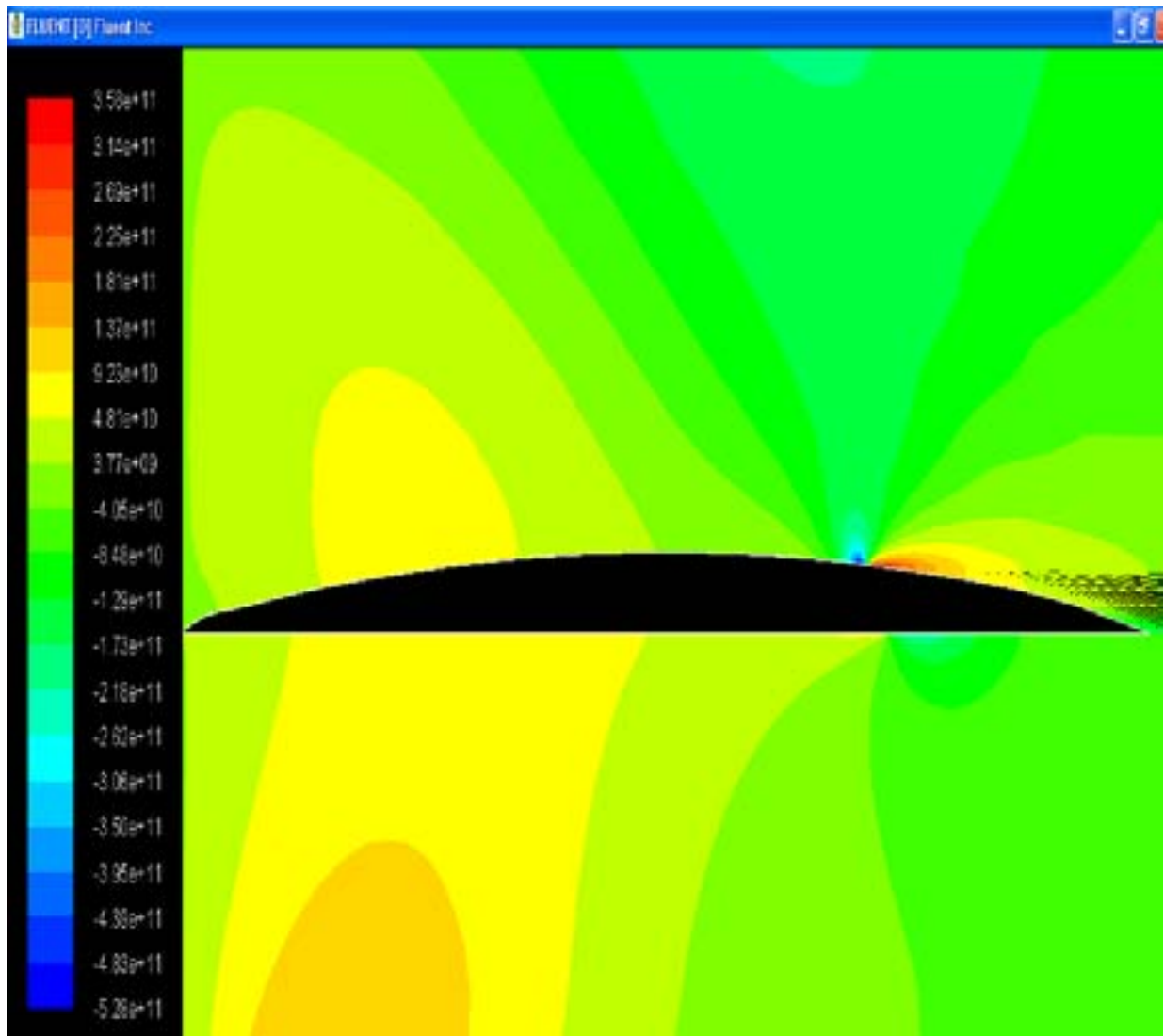


Figure 18:

2

Temperature (°C)	Density (kg/ m 3)		Kinematic viscosity (m 2 /s x 10 6)	
	Fresh water	Salt water	Fresh water	Salt water
0	999.8	1028.0	1.787	1.828
10	999.6	1026.9	1.306	1.354
20	998.1	1024.7	1.004	1.054
30	995.6	1021.7	0.801	0.849

Figure 19: Table 2 :

3

	sea water (Carlton, 2007)	
Temperatur e (°C)	0.01 5	10 15 20 25 30
Fresh water, P v (Pa)	611 872 1228 1704 2377 3166 4241	
Sea water, P v (Pa)	590 842 1186 1646 2296 3058 4097	

Figure 20: Table 3 :

